NOTES AND CORRESPONDENCE

Supplement to "Numerical Simulation of Lee-Wave Events over the Pyrenees"

By Takehiko Satomura[1]

Meteorological Research Institute 1-1, Nagamine, Tsukuba, Ibaraki 305, Japan

(Manuscript received 21 July 1995, in revised form 1 December 1995)

Abstract

The vertical flux of horizontal momentum by three-dimensional mountain waves is examined using a linear theory. Analytic solutions for two different wind directions are obtained using numerical Fourier analysis. Although the mountain examined in this note is a fairly two-dimensional one, the results show that, at the tropopause level, the momentum flux greatly decreases to 1/4∼1/3 of its near-surface value even over the center area of the mountain when the mean wind crosses the mountain at 45 degrees. It is also suggested that the decrease of the momentum flux observed in IOP-3 of PYREX is caused by both the finite length of the Pyrenees mountains and the slant attack angle of the mean wind.

1. Introduction

In this note, the vertical flux of horizontal momentum by linear gravity waves over three-dimensional mountains will be calculated to clarify the effects of the wind direction and of the finite length of the mountains on the vertical profile of the flux.

In a previous paper (Satomura and Bougeault, 1994: hereafter SB94), the mountain waves observed in the two lee-wave events during the PYREX program (Bougeault *et al.*, 1990, 1993) were simulated by a two-dimensional non-hydrostatic model. The model used in SB94 simulated well the wavelength, the amplitude and the position of the observed lee waves, and they indicated that the lee waves observed in the third intensive observation period (IOP-3) were excited by non-linear wave-wave interactions of long mountain waves. In spite of these agreements, the vertical distribution of the momentum flux by the simulated mountain waves did not agree with the observation: the simulated flux was almost constant through the troposphere, whereas the observation showed rapid decrease of the absolute values.

Under the stationary and two-dimensional conditions, the vertical flux of horizontal momentum by small amplitude gravity waves must be constant in inviscid fluids without a critical level (Eliassen and Palm, 1960). Since the long and vertically-propagating mountain wave (called a principal wave in SB94) did not produce strong turbulence in IOP-3 during the PYREX by the simulation (neither by observation), the above results of SB94 were consistent with that non-acceleration theorem. On the other hand, the three-dimensional time-dependent model of Beau (1992) and Bougeault *et al.* (1993) simulated the momentum flux well. Considering above results, it was suggested in SB94 that a reason giving rise to the disagreement about the momentum flux is the three-dimensionality of the environmental field such as the mountain shape and the direction of the mean wind in the real atmosphere.

Mountain waves over three-dimensional elliptical mountains have been examined by several studies. Blumen and Dietze (1981, 1982) solved mountain-wave equations over multiple elliptical mountains in a shear flow and calculated the momentum flux. Smith (1989) showed a diagram of critical mountain height for stagnation as a function of horizontal aspect ratio using the linear theory. His diagram indicates that mountains of high aspect ratio (> 5) act as a two-dimensional wall. Using a hydrostatic numerical model, Stein (1992) examined non-linear effects on critical mountain height for stagnation and confirmed the diagram of Smith (1989).

1 Present affiliation: Dept. of Geophys., Kyoto Univ. Kitashirakawa Oiwakecho, Sakyo-ku, Kyoto 606-01, Japan

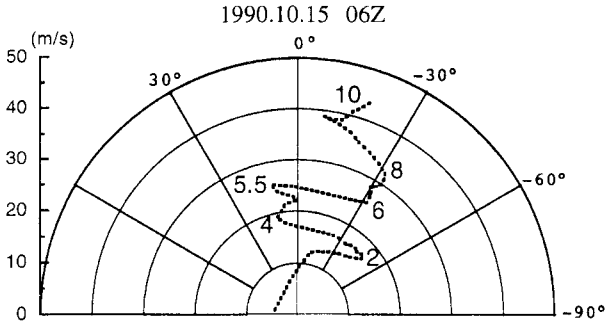

Fig. 1. Hodograph of the horizontal wind at 0600 UTC 15 October 1990 at Zaragoza, Spain. The angle 0° indicates that the wind crosses the Pyrenees mountain at right angles from Spain to France side. Numbers labelled on the dotted line show the height in km.

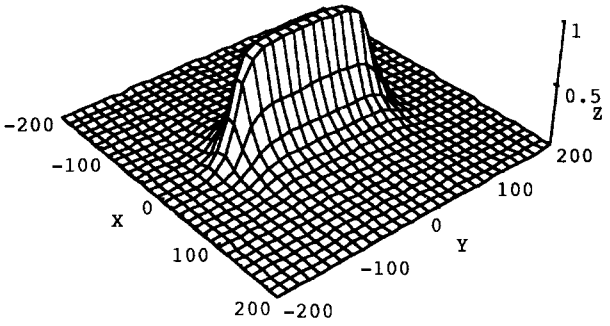

Fig. 2. Bird's-eye view of the bottom topography with $a = b = 20$ and $L = 100$.

According to the diagram of Smith (1989), the Pyrenees are fairly two-dimensional mountains because the Pyrenees have high aspect ratio of about 5 or more: the scale of the Pyrenees is about 350 km×70 km at 1000 m height contour (see Fig. 1b in SB94 for example). This expectation is contradictory to the suggestion in SB94. Above studies, however, examined mountain waves under the condition that the mean wind approaches the mountain at right angles, which rarely occurs in the real atmosphere.

In IOP-3, indeed, the air flowed over the Pyrenees at other than right angles in the most part of the troposphere, as shown in Fig. 1. This wind hodograph at an upstream-side observation station, Zaragoza, Spain, reveals the fact that the air approached the Pyrenees at an angle of ~ -30 degrees (nearly south-westerly) except at 4~5.5 km height. In particular, the attack angle was nearly -45 degrees at 2 km height where the peaks of the Pyrenees mountains stick out. Though the mountain waves in a slant mean wind will have intermediate characteristics between the cases where the wind crosses the mountain at the attack angle of 0° and of ±90°, quantitative discussions of such waves have not yet been made.

Therefore, in this note, attention will be given to cases where the uniform mean wind approaches the mountain aslant. Also, a cause of the observed decrease of the momentum flux will be given.

2. Basic equations

Consider the steady flow of a vertically half-unbounded, stratified Boussinesq fluid, over small-amplitude topography $z = h(x, y)$. The perturbations to the vertically uniform background wind, pressure and potential temperature fields are described by the linearized equations:

$$U\frac{\partial u'}{\partial x} + V\frac{\partial u'}{\partial y} + c_p\Theta_{00}\frac{\partial \pi'}{\partial x} = 0, \tag{2.1}$$

$$U\frac{\partial v'}{\partial x} + V\frac{\partial v'}{\partial y} + c_p\Theta_{00}\frac{\partial \pi'}{\partial y} = 0, \tag{2.2}$$

$$U\frac{\partial w'}{\partial x} + V\frac{\partial w'}{\partial y} + c_p\Theta_{00}\frac{\partial \pi'}{\partial z} = g\frac{\theta'}{\Theta_{00}}, \tag{2.3}$$

$$U\frac{\partial \theta'}{\partial x} + V\frac{\partial \theta'}{\partial y} + w'\frac{d\Theta_0}{dz} = 0, \tag{2.4}$$

$$\frac{\partial u'}{\partial x} + \frac{\partial v'}{\partial y} + \frac{\partial w'}{\partial z} = 0, \tag{2.5}$$

where $(U, V, 0)$ and (u', v', w') are the constant mean wind velocity and the perturbation wind velocity in the (x, y, z) direction, respectively; c_p is the specific heat for constant pressure; θ' is the perturbation potential temperature; Θ_{00} and $d\Theta_0/dz$ are the reference potential temperature and the background vertical potential temperature gradient, respectively; $\pi' = (p/p_{00})^{R/C_p} - \Pi$ is the perturbation Exner function, in which p is the pressure, p_{00} is the reference pressure, R is the dry gas constant and

$$c_p\Theta_{00}\frac{d\Pi}{dz} = -g\left(1 - \frac{\Theta_0}{\Theta_{00}}\right).$$

Introducing scale parameters of the velocity and the time as U_0 and $1/N$, respectively, variables are non-dimensionalized as:

$$(x, y, z) = (\hat{x}, \hat{y}, \hat{z})l_s^{-1},$$
$$(U, V, u', v', w') = (\hat{U}, \hat{V}, \hat{u}, \hat{v}, \hat{w})U_0,$$

where

$$N^2 = \frac{g}{\Theta_0}\frac{d\Theta}{dz},$$

is the square of the buoyancy frequency and

$$l_s = \frac{N}{U_0}$$

is the Scorer parameter of the uniform atmosphere.

The equations (2.1)~(2.5) can be reduced to a single non-dimensionalized equation for the vertical velocity:

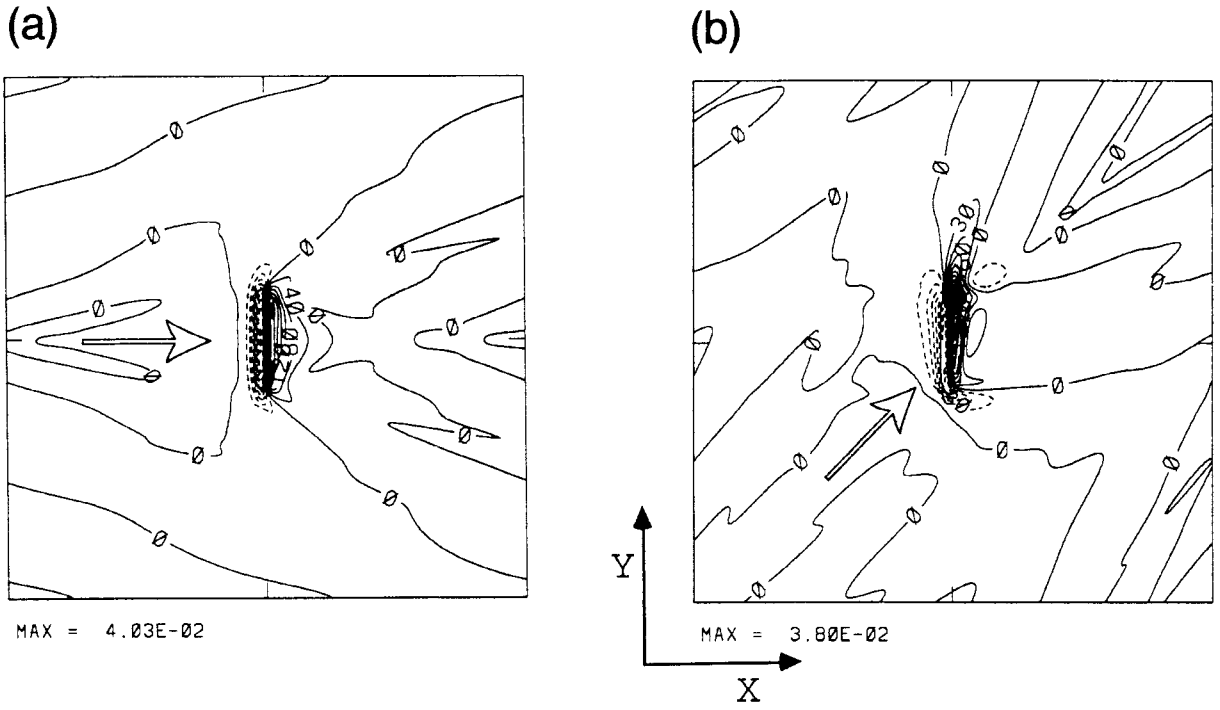

Fig. 3. Perturbation vertical velocity $\hat{w}$ at $\hat{z} = 0.4 \times 2\pi$ for (a) $\alpha = 0$, and (b) $\alpha = \pi/4$. Solid and dashed lines indicate positive and negative values, respectively. The contour interval is (a) 20×10^{-4} and (b) 30×10^{-4}. The white arrows indicate mean wind directions. The mountain is located at the center of the domain.

$$(kU+lV)^2 w_{zz} - (k^2+l^2)\{(kU+lV)^2 - 1\}w = 0, \quad (2.6)$$

where the subscript z indicates z-derivative and we assume the perturbations to be represented as a double Fourier integral

$$\hat{w}(x,y,z) = \int\int_{-\infty}^{+\infty} w(k,l,z) e^{i(kx+ly)} dk dl.$$

With N^2 taken as constant and the linearized lower boundary condition

$$w(k,l,0) = i(kU + lV)h(k,l), \quad (2.7)$$

the solution to (2.6) is written in physical space as:

$$\hat{w}(x,y,z) = \int\int_{-\infty}^{+\infty} i(kU+lV)h(k,l) e^{imz} e^{i(kx+ly)} dk dl, \quad (2.8)$$

where

$$m^2 = \frac{(k^2+l^2)\{1-(kU+lV)^2\}}{(kU+lV)^2}. \quad (2.9)$$

For $m^2 < 0$ the positive imaginary root of (2.9) must be chosen to eliminate the non-physical growth of the disturbance amplitude with height, and for $m^2 > 0$ the sign of m must be chosen to be the same as the sign of $(kU + lV)$ in order to satisfy the radiation condition aloft (see Smith, 1980, for $V = 0$).

To examine the effects of the three-dimensionality of a nearly two-dimensional mountain range, a "table-shaped" mountain

$$\hat{h} = \frac{1}{1+(\hat{x}/a)^2} \times \frac{\left\{1+\tanh\left(\frac{\hat{y}+d}{b}\right)\right\}\left\{1+\tanh\left(-\frac{\hat{y}-d}{b}\right)\right\}}{\{1+\tanh(d/b)\}^2}, \quad (2.10)$$

is considered, where the non-dimensional parameters are $a = b = 20$ and $d = 100$. These parameters give a long slender mountain range as shown in Fig. 2. Applying the Score parameter observed in the middle troposphere during the IOP-3 of PYREX ($\sim$0.6 km^{-1}; SB94), this mountain has half widths of 30 km in the crossing-mountain direction and 150 km in the along-mountain direction. These values are equivalent to the Pyrenees mountains, and it is expected to behave like a two-dimensional wall because of its high aspect ratio.

When the wind crosses the mountain at right angles, mountain waves generated by the above table-shaped mountain show the best two-dimensionality. However, it rarely occurs in the real atmosphere. During the IOP-3 of PYREX also, the wind approached the Pyrenees mountains aslant as shown in Fig. 1. Therefore we will examine two cases of

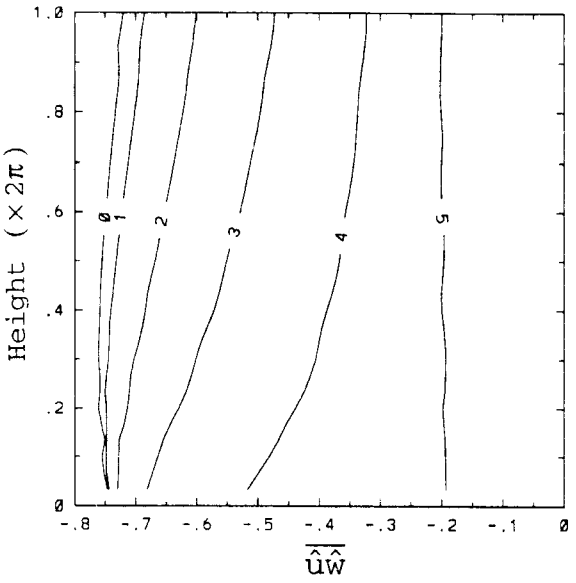

Fig. 4. Vertical profile of the non-dimensional vertical momentum flux M_X at $\hat{y} = 0$ (line number $n = 0$), 20 ($n = 1$), 40 ($n = 2$), 60 ($n = 3$), 80 ($n = 4$) and 100 ($n = 5$) for $\alpha = 0$. The ordinate is the non-dimensional height divided by 2π.

attack angles of the wind: $\alpha \equiv \tan^{-1}(V/U) = 0$ and $\pi/4$.

In the following sections, analytical solutions are obtained using a fast Fourier transform (FFT) algorithm in the horizontal directions at specified heights. This implies the horizontally periodic nature in a square domain. The sides of the domain in this study are 1024 × 1024 in the non-dimensional units divided by 256 grids for the discrete FFT. The effects of cyclic side boundary conditions on the momentum flux are negligible because the solutions do not change practically in a wide domain of 2048 × 2048 sides.

3. Results

As shown in Fig. 3a, the gravity waves over the table-shaped mountain for $\alpha = 0$ are not much different from those over a circular mountain (*ex.* Smith, 1980). On the other hand, when $\alpha = \pi/4$ (Fig. 3b), we notice waves are generated over two distinctive areas: the lower-left corner of the mountain which is the leading up-slope for this wind direction, and the upper-right corner which is the final down-slope. The wave-train is less remarkable than that for $\alpha = 0$.

Vertical profiles of the non-dimensional momentum flux,

$$M_X(\hat{y}, \hat{z}) \equiv \overline{\hat{u}\hat{w}} = \int_{-L_X/2}^{L_X/2} \hat{u}\hat{w} d\hat{x}, \qquad (3.1)$$

where L_X is the domain length in the x-direction, are calculated at $\hat{y} = 0$ (at the center of the mountain), 20, 40, 60, 80 and 100 (at the shoulder of the mountain) for $\alpha = 0$ are shown in Fig. 4. Since the non-dimensional height $1.0 \times 2\pi$ corresponds ~10 km applying l_S ~0.6 km^{-1} observed in IOP-3 of PYREX (SB94), Fig. 4 and following corresponding figures show vertical variation of M_X through the troposphere. It is shown in Fig. 4 that M_X decreases only 5 ~20 % near the center of the mountain (line number n= 0 ~ 2). Since the momentum flux of steady two-dimensional linear mountain waves must be constant in the vertical direction, this small change of M_X indicates that our table mountain has nearly two-dimensional characteristics near the center if $\alpha = 0$. In the off-center area, however, M_X decreases to about 40 % (n=3) even in this case.

The momentum flux M_X when $\alpha = \pi/4$ is shown in Fig. 5. In this case, M_X at the top of the domain is as small as 1/4 ~ 1/3 of its value at the lowest altitude near the center of the mountain (n= 0, ±1 and ±2) where the waves are nearly two-dimensional if $\alpha = 0$. Further, M_X is not symmetric with $y = 0$. Leaving toward the upstream direction (*i.e.* $\hat{y} < 0$) from the center of the mountain, the absolute value $|M_X|$ tends to decrease (Fig. 5a). In contrast, it tends to increase on the other side of the mountain ($\hat{y} > 0$) as shown in Fig. 5b and to be nearly constant in the vertical. The increase of $|M_X|$ toward the downstream direction is most likely caused by gravity waves generated upstream side of the mountain summed up in the downstream area.

4. Discussion

Two features are obvious from the results. Firstly, the magnitude of the momentum flux at the top of the domain is about 1/4 ~ 1/3 of the near surface value over the center of the table-shaped mountain when $\alpha = \pi/4$. This decrease of the flux is nearly the same as that over a circular bell-shaped mountain. One may, however, notice that the integration line in M_X (*i.e.*, x-axis) is not parallel to the wind direction and suppose this would cause the reduction of M_X. To clarify this point, the horizontal distribution of $\hat{u}\hat{w}$ at $\hat{z} = 0.8 \times 2\pi$ is shown in Fig. 6. Because the momentum flux M_X is the line integration of $\hat{u}\hat{w}$, it will remain large at this height even if the integration line is not parallel to the wind direction when $\alpha = 0$ (Fig. 6a). When $\alpha = \pi/4$ (Fig. 6b), however, the flux will be small near the center of the mountain even if integration line is parallel to the wind direction. Indeed, the results of the line integration reveal that the momentum flux decreases at the top of the domain to about 80 % of the near surface value if $\alpha = 0$ and the integration line crosses the wind at an angle of $\pi/4$, but the momentum flux decreases to about 30 % of the near surface value if $\alpha = \pi/4$ and the integration line is parallel to the

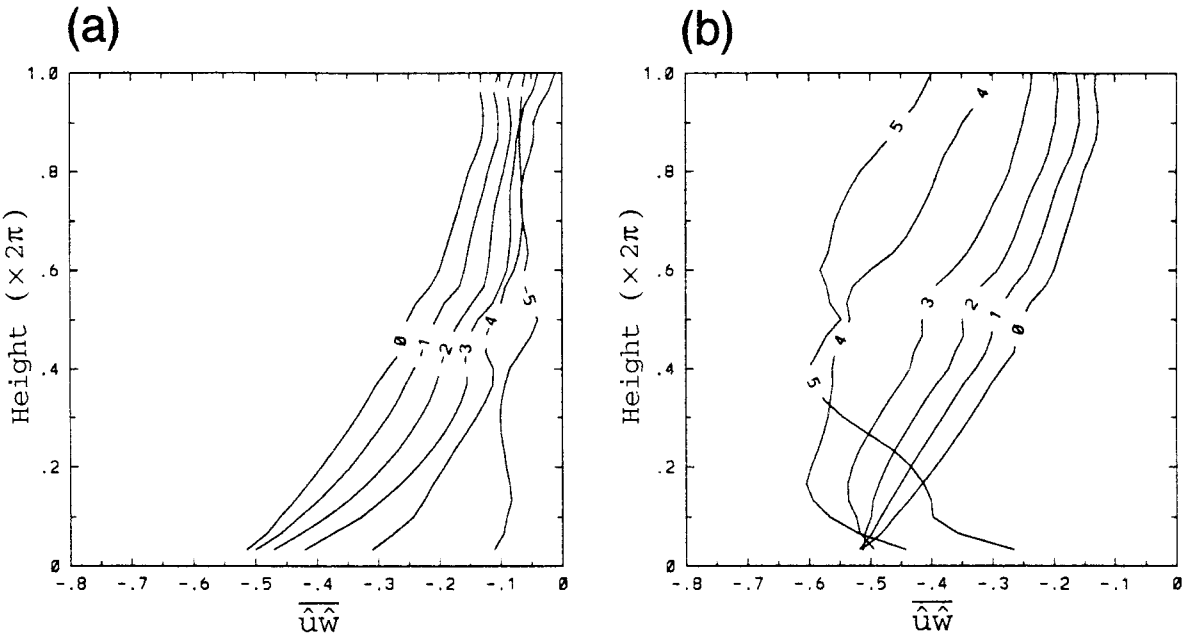

Fig. 5. (a) Same as Fig. 4, except at $\hat{y} = 0$ ($n = 0$), -20 ($n = -1$), -40 ($n = -2$), -60 ($n = -3$), -80 ($n = -4$) and -100 ($n = -5$) for $\alpha = \pi/4$. (b) Same as Fig. 4, except for $\alpha = \pi/4$.

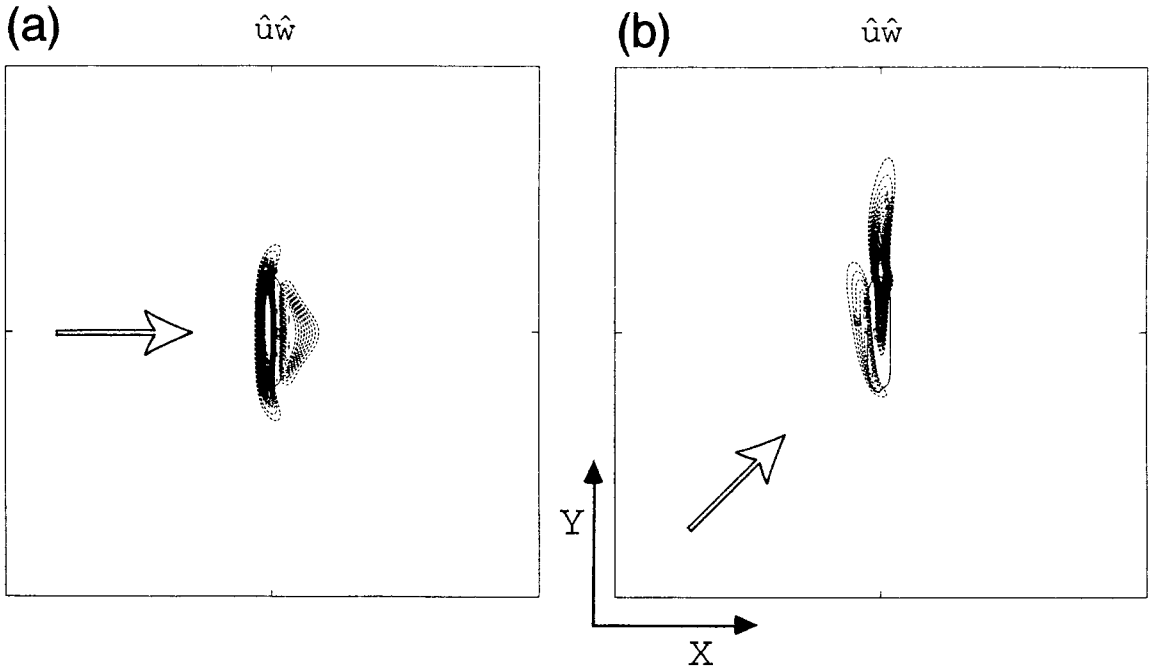

Fig. 6. Same as Fig. 3, except for the correlation $\hat{u}\hat{w}$ at $\hat{z} = 0.8 \times 2\pi$. The contour interval is 5×10^{-4}.

wind (not shown). Therefore, the non-parallel integration line of M_X is not the cause of the reduction of $|M_X|$, but the shift of the maximum of $-\hat{u}\hat{w}$ to the downstream direction along the mountain causes this reduction.

One may further notice that the width of the mountain in the cross-stream direction decreases to $\sin\alpha$ and may suppose that this causes the reduction of $|M_X|$ when $\alpha = \pi/4$. This possibility is also denied by calculations with a deformed mountain (the extent is shortened by $\sin(\pi/4)$ and the half-width is elongated by $1/\sin(\pi/4)$) and $\alpha = 0$, because $|M_X|$ at the top of the domain differs only a small amount (15 %) from that at the bottom (not shown).

Therefore, we conclude that both the finite length of the mountain and the slant attack angle of the mean wind ($\alpha \neq 0$) mainly cause of the decrease of the momentum flux. On the other hand, the di-

rection of the line of flux integration plays a minor role on it. Consequently, these results suggest the observed reduction of the momentum flux (to about 1/3 of that in lower altitude) in IOP-3 (Bougeault *et al.*, 1993; SB94) was mainly caused by both the finite length of the Pyrenees mountain and the slant attack angle of the mean wind.

The second feature is that even for the gravity waves generated by fairly two-dimensional mountains as the Pyrenees one should not use the line averaged flux M_X as an indicator of the deposition of wave momentum. The important quantity for the momentum budget is, as well known, the momentum flux averaged in a horizontal area,

$$M_S \equiv \int\int_S \overline{\hat{u}\hat{w}} d\hat{x} d\hat{y}, \tag{4.1}$$

where $S = L_X \times L_Y$ is a horizontal plane of the domain and L_Y is the domain length in the y-direction. Not the line-averaged momentum flux M_X but this area-averaged flux M_S is constant for stationary three-dimensional mountain waves in a uniform flow[2] because the non-acceleration theorem (Eliassen and Palm, 1960) holds for M_S. Therefore, the vertical variations of the line-averaged momentum flux M_X shown in Fig. 5 do not indicate the overall horizontal momentum change.

This point is evident when the mountain shape is highly three-dimensional (circular bell-shaped mountain, for example). Nevertheless, it is noteworthy that M_X greatly decreases over the fairly two-dimensional mountains of large horizontal aspect ratio (> 5) if the wind does not cross the mountain at the right angles. This happens frequently in the real atmosphere. In field experiments, the momentum flux in the upper air is observed by aircraft which is a fundamentally line-averaged momentum flux. Therefore, one must pay great attention to using the observed momentum flux profile to estimating the whole effects of the mountainous area on the atmosphere.

5. Conclusions

The vertical flux of horizontal momentum by gravity waves over a table-shaped mountain was computed using linear equations. The main result is that the momentum flux at the top of the domain (~10 km height) is about $1/4 \sim 1/3$ of the near surface value when the wind crosses the mountain with the angle of $\pi/4$. The flux also shows the strong asymmetry respect to the center of the mountain in this case. Further, it was suggested that the decrease of momentum flux observed in IOP-3 of PYREX was mainly caused by both the finite length of the Pyrenees mountains and the slant attack angle of the mean wind.

Acknowledgments

The author greatly acknowledges helpful discussions with the member of Appl. Meteor. Res. Dep. of MRI, and also useful comments of anonymous reviewers.

The PYREX experiment is a cooperative program supported by Météo-France, the Spanish Institute for Meteorology, CNRS/INSU, CNES, EDF, Région Midi-Pyrénées and DLR.

References

Beau, I., 1992; Evaluation des paramétrisation de l'effet orographique sous-maille dans les modèle de circulation générale à l'aide de PERIDOT 10 km, *Note de Travaille de l'ENM*, ENM, CNRM, 153 pp.

Blumen, W. and S.C. Dietze, 1981; An analysis of three-dimensional mountain waves in a stratified shear flow, *J. Atmos. Sci.*, **38**, 1949–1963.

Blumen, W. and S.C. Dietze, 1982; An analysis of three-dimensional mountain waves in a stratified shear flow: Part II, *J. Atmos. Sci.*, **39**, 2712–2720.

Bougeault, P., A. Jansa, B. Benech, B. Carrisimo, J. Pelon and E. Richard, 1990; Momentum budget over the Pyrénées: The PYREX experiment, *Bull. Amer. Meteor. Soc.*, **71**, 806–818.

Bougeault, P., A. Jansa, J.L. Attié, I. Beau, B. Benech, R. Benoit, P. Bessemoulin, J.L. Caccia, J. Campins, B. Carrisimo, J.L. Champeaux, M. Crochet, A. Druilhet, P. Durand, A. Elkhalfi, P. Flamant, A. Genoves, M. Georgelin, K.P. Hoinka, V. Klaus, E. Koffi, V. Kotroni, C. Mazaudier, J. Pelon, M. Petitdidier, Y. Pointin, D. Puech, E. Richard, T. Satomura, J. Stein and D. Tannhauser, 1993; The atmospheric momentum budget over a major mountain range: First results of the PYREX field program, *Annales geophysicae*, **11**, 395–418.

Eliassen, A. and E. Palm, 1960: On the transfer of energy in stationary mountain waves, *Geofys. Publ.*, **22**, 1–23.

Satomura, T. and P. Bougeault, 1994; Numerical simulation of lee wave events over the Pyrenees, *J. Meteor. Soc. Japan*, **72**, 173–195.

Smith, R.B., 1980; Linear theory of stratified hydrostatic flow past an isolated mountain, *Tellus*, **32**, 348–364.

Smith, R.B., 1989; Mountain-induced stagnation points in hydrostatic flow, *Tellus*, **41A**, 270 274.

Stein, J., 1992; Contribution à l'étude des règimes hydrostatiques d'écoulements orographiques, Ph. D. Thesis, Univ. Paul Sabatier, Toulouse, France.

2 We also confirmed that M_S is constant in our calculation.

ピレネー山脈における風下波の数値シミュレーションに関する補遺

里村雄彦[1]
（気象研究所）

線形3次元山岳波による運動量の鉛直輸送について、解析解の数値評価を行うことによって調べた。地形として2次元性の良い山脈状のものを用い、平均風が山脈に直角に当たる場合と斜め45度から吹く場合の2種類について計算した。

その結果、平均風が斜め45度で山脈に当たる場合には、対流圏界面付近の運動量フラックスは山脈の中心付近でさえ地表近くの1/4から1/3に減ることが判った。また、PYREXのIOP-3で観測された運動量フラックスの減少は、ピレネー山脈が有限の横幅しかないという3次元性と平均風向が山脈に直角ではなかったということとが主な原因であると示唆された。

[1]現所属：京都大学大学院理学研究科地球物理学教室